UC Santa Barbara

UC Santa Barbara Previously Published Works

Title

Stress relaxation rates of myocardium from failing and non-failing hearts.

Permalink

https://escholarship.org/uc/item/10h154xn

Authors

Gionet-Gonzales, Marissa

Gathman, Gianna

Rosas, Jonah

et al.

Publication Date

2024-12-31

DOI

10.1007/s10237-024-01909-4

Peer reviewed

eScholarship.org Powered by the California Digital Library
University of California

Biomechanics and Modeling in Mechanobiology (2025) 24:265–280
https://doi.org/10.1007/s10237-024-01909-4

ORIGINAL PAPER

Stress relaxation rates of myocardium from failing and non-failing hearts

Marissa Gionet-Gonzales[1,3] · Gianna Gathman[1] · Jonah Rosas[4] · Kyle Y. Kunisaki[3] · Dominique Gabriele P. Inocencio[3] · Niki Hakami[3] · Gregory N. Milburn[2] · Angela A. Pitenis[4] · Kenneth S. Campbell[2] · Beth L. Pruitt[1,3] · Ryan S. Stowers[1,3]

Received: 23 July 2024 / Accepted: 6 November 2024 / Published online: 31 December 2024
© The Author(s) 2024

Abstract

The heart is a dynamic pump whose function is influenced by its mechanical properties. The viscoelastic properties of the heart, i.e., its ability to exhibit both elastic and viscous characteristics upon deformation, influence cardiac function. Viscoelastic properties change during heart failure (HF), but direct measurements of failing and non-failing myocardial tissue stress relaxation under constant displacement are lacking. Further, how consequences of tissue remodeling, such as fibrosis and fat accumulation, alter the stress relaxation remains unknown. To address this gap, we conducted stress relaxation tests on porcine myocardial tissue to establish baseline properties of cardiac tissue. We found porcine myocardial tissue to be fast relaxing, characterized by stress relaxation tests on both a rheometer and microindenter. We then measured human left ventricle (LV) epicardium and endocardium tissue from non-failing, ischemic HF and non-ischemic HF patients by microindentation. Analyzing by patient groups, we found that ischemic HF samples had slower stress relaxation than non-failing endocardium. Categorizing the data by stress relaxation times, we found that slower stress relaxing tissues were correlated with increased collagen deposition and increased α-smooth muscle actin (α-SMA) stress fibers, a marker of fibrosis and cardiac fibroblast activation, respectively. In the epicardium, analyzing by patient groups, we found that ischemic HF had faster stress relaxation than non-ischemic HF and non-failing. When categorizing by stress relaxation times, we found that faster stress relaxation correlated with Oil Red O staining, a marker for adipose tissue. These data show that changes in stress relaxation vary across the different layers of the heart during ischemic versus non-ischemic HF. These findings reveal how the viscoelasticity of the heart changes, which will lead to better modeling of cardiac mechanics for in vitro and in silico HF models.

Keywords Viscoelasticity · Stress relaxation · Mechanobiology · Heart failure

1 Introduction

Viscoelasticity allows stress within the heart to dissipate over time. Previous studies based on in vivo imaging suggest that the viscoelasticity of the heart changes during HF (Hess et al. 1979; Pislaru et al. 2014). However, direct ex vivo viscoelastic measurements of human HF and non-failing tissue are lacking. Further, how tissue remodeling due to HF influences cardiac viscoelasticity remains unknown.

✉ Beth L. Pruitt
blp@ucsb.edu

✉ Ryan S. Stowers
rstowers@ucsb.edu

[1] Bioengineering, University of California, Santa Barbara, Santa Barbara, United States

[2] Internal Medicine, University of Kentucky, Lexington, United States

[3] Present Address: Mechanical Engineering, University of California, Santa Barbara, Santa Barbara, United States

[4] Materials, University of California, Santa Barbara, Santa Barbara, United States

Box: Viscoelasticity defined

Viscoelasticity

Viscoelastic materials exhibit both a viscous and elastic response when compressed by a force (**A**). The resulting material deformation can be defined as strain (**1**), and the force can be converted to stress (**2**), where L_o is the initial sample length, L_1 is the sample length during indentation, and Δ is the difference between the two.

(**1**) Strain = $\frac{\Delta}{L_o}$ (**2**) Stress = $\frac{\text{Force}}{\text{Area}}$

Stress Relaxation

In a stress relaxation test, a constant strain (**B**) is exerted on the material and the subsequent stress decay (**C**) is measured. We characterize the material relaxation by calculating the $\tau_{1/2}$. The $\tau_{1/2}$ indicates the time at which the stress reaches half its initial maximum value.

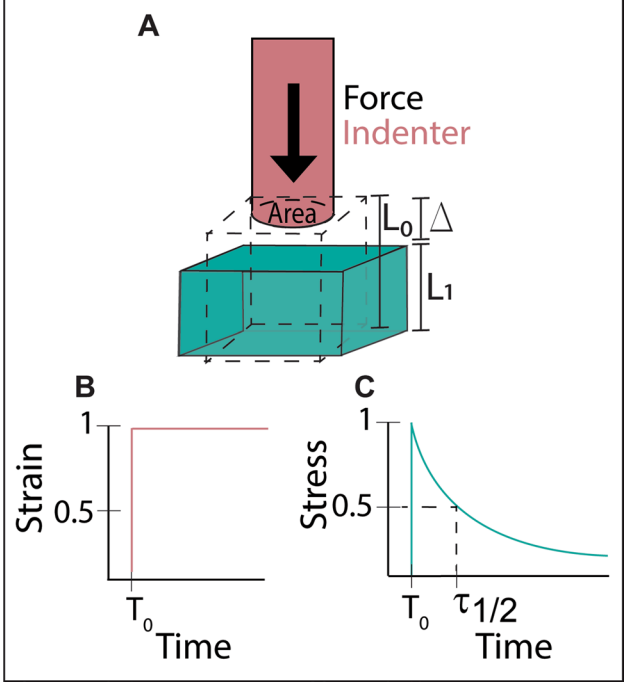

The heart's functional performance is directly linked to its viscoelasticity. Viscoelasticity regulates cardiac wall compliance, which in turn controls the amount of blood that can fill the chamber (Magder 2016). The LV filling capacity is increased in faster relaxing cardiac tissue and decreased in slower relaxing cardiac tissue (Caporizzo and Prosser 2021). If the heart does not relax fast enough for adequate filling, the subsequent decrease in LV output will cause an increase in end diastolic pressure. Increased diastolic pressure results in increased stress on the heart walls, leading to a variety of complications. In the short term, this increased pressure leads to circulatory congestion, causing edema (Gandhi et al. 2001), long term, high blood pressure can damage cells and lead to diastolic HF (Zile and Brutsaert 2002).

At the cellular level, viscoelasticity regulates cell proliferation (Bauer et al. 2017), spreading (Gong et al. 2018), differentiation (Charrier et al. 2018) and survival (Sacco et al. 2024) in a number of cell types, including fibroblasts (Chaudhuri et al. 2015), stem cells (Chaudhuri et al. 2016; Cameron et al. 2011) and cancer cells (Fan et al. 2024). To date, there has been limited investigation into how substrates with different relaxation rates influence cardiomyocytes (CMs). CMs are mechanosensitive; in vitro experiments show that they can modulate their morphology and function in response to stiffness (Boothe et al. 2016; Chang et al. 2021; Corbin et al. 2019; Körner et al. 2021) and stretch (Wong et al. 2018; Rysä et al. 2018). Therefore, CMs are likely influenced by the viscoelastic cues of their substrate.

Viscoelastic substrates, including decellularized extracellular matrix (ECM) (Hunter et al. 2022; Ott et al. 2008) and viscoelastic hydrogels, such as Matrigel, collagen and fibrin (Bakunts et al. 2008; Roshanbinfar et al. 2024; Kaiser et al. 2019), have been used for CM culture. However, these studies did not measure the viscoelasticity of their materials or investigate the effect of viscoelasticity independently of other parameters. Alternatively, biomaterials can be engineered to allow for tunability of viscoelasticity. Notably, one study found that CMs action potential duration increased after being cross-linked in a viscoelastic hydrogel compared to the cells before cross-linking (Hegyi et al. 2021). Another study showed increases in CM spreading, YAP localization and sarcomere organization with increasing storage modulus; however, they also saw an increase in their loss modulus and loss factor (tanδ), in their dynamic hydrogels (Corbin et al. 2019). Since there were changes in both elastic and viscoelastic behavior within their hydrogels, the influence of viscoelasticity alone is hard to determine. Several other studies use viscoelastic engineered biomaterials for CMs, but are unable to verify that the viscoelasticity of their material is physiologically accurate due to the lack of reliable tissue measurements (Corbin et al. 2019; Roman et al. 2021; Schmitt et al. 2022). Cell behavior can change substantially depending on the degree of substrate viscoelasticity (Chaudhuri et al. 2016), motivating the need for cardiac viscoelastic measurements to aid in the development of cardiac biomaterials with physiologically relevant stress relaxation.

Computational models of the mechanical behavior of the heart would also benefit from experimental measurements of viscoelastic tissue mechanics (Land et al. 2017). Several computational studies do not incorporate the effects of

viscoelasticity (Willems et al. 2024; Mendiola et al. 2023; Vetter and McCulloch 1998). Studies that do investigate viscoelasticity, through incorporating experimental stress relaxation data, fail to agree on the role and importance of viscoelasticity in computational models. One reason for this disagreement is because it is unclear if the time scale and magnitude of cardiac tissue viscoelasticity are relevant at a heartbeat scale; our work will help to answer this question (Tikenoğulları et al. 2022; Hassan et al. 2012). One computational study concluded that viscoelasticity plays an important role in the cardiac relaxation phase, with increasing importance during disease conditions (Zhang et al. 2023). Through finite element analysis, the authors found that their viscoelastic model had reduced stroke volume compared to an elastic model. Unfortunately, their model did not investigate how changing viscoelastic parameters, to mimic disease progression, influenced cardiac function. Our results address this gap in knowledge, by providing viscoelastic measurements from failing and non-failing human hearts.

To accomplish this, we conducted stress relaxation tests on porcine cardiac tissue and human non-failing cardiac tissues, as well as ischemic HF, and non-ischemic HF. We characterized fibrosis and adipose content within the endocardium (inner layer) and epicardium (outer layer), of the heart and correlated these with the relaxation rate. Our viscoelastic measurements will aid in the development of improved engineered biomaterials and computational modeling of the heart.

2 Materials and methods

2.1 Porcine tissue acquisition and storage

We acquired porcine hearts to establish a baseline measurement of the relaxation of cardiac tissue. Porcine hearts are a useful approximation for human hearts, due to their similarity in structure, size and function (Rawat et al. 2023). Frozen, formaldehyde-free porcine hearts were acquired from VWR (cat# 470,330-138), or local markets (Santa Barbara Meat Co). Hearts were stored at − 20 °C, and thawed at 4 °C for 12 h before mechanical testing was performed at room temperature. Once thawed, the LV was isolated using a scalpel. The LV wall was then cut with an 8 mm biopsy punch to produce a cylindrical core of tissue. The tissue core was then trisected into equal sections for mechanical testing. These sections were labeled as the inner layer (endocardium), middle layer (mid-myocardium) and outer layer (epicardium). Measuring the different layers independently is important since significant differences in the collagen content between the different layers can be indicative of heart disease (Haynes et al. 2014).

For mechanical measurements on decellularized tissue, we cut thawed porcine tissue into ~ 15 × 5 mm sections of 2–3 mm thickness from the LV of a porcine heart. The sections were placed in 1% sodium dodecyl sulfate (SDS) on a plate shaker at 60 rpm at 4 °C for 4 days. After this treatment, the tissues were washed in 1X DPBS for 30 min to remove the remaining SDS. These decellularized tissues were then immediately subjected to mechanical testing.

2.2 Human tissue acquisition and storage

Human myocardium was procured from patients receiving cardiac transplants or from organ donors at the University of Kentucky. Patients, or their legally authorized representatives, provided informed consent, and all procedures were approved by the University of Kentucky Institutional Review Board (protocol 46,103). All the patients who received heart transplants had advanced HF. Hearts from organ donors were procured for research when the organ could not be used for transplant. Details of the procurement have been published (Blair et al. 2016). Samples of approximately 1 g were flash frozen in liquid nitrogen and shipped to UCSB on dry ice. The endocardium and epicardium were provided for each patient. Once received at UCSB, samples were stored at - 80 °C until day of testing. On the day of testing, samples were submerged in PBS to thaw for 5 min. Once thawed, a small flat section was cut off for testing, approximately 3–5 mm thick, with a surface of at least 3 × 3 mm.

2.3 Mechanical characterization

Porcine cardiac tissue was measured using an ARES G2 rheometer (TA Instruments) with 8 mm parallel plates. First, an oscillatory shear strain test was conducted at 1% strain and an angular frequency of 6.28 rad/s to measure the storage and loss moduli of the tissue. Then, a stress relaxation test was performed, where an instantaneous 15% shear strain was applied to the sample and the resulting relaxation modulus was measured.

The viscoelasticity of human and porcine myocardium was measured using a custom-built microindenter (Krick et al. 2012; Urueña et al. 2018; Chau et al. 2022, 2023; Atkins et al. 2024). A 1.5 mm diameter quartz flat punch probe of 8 mm height was used for indentation. This allowed us to analyze smaller samples than would not have been possible using the rheometer. The lateral fixture had a spring constant of $K_n = 437.8$ µN/um, and the normal fixture had a spring constant of $K_n = 184.6$ µN/nm. The tissue was indented rapidly (2000 µm/s) to 10% of the sample thickness, and the indentation was held for at least 30 s, or until $\tau_{1/2}$, or half the initial maximum stress value, was reached. To confirm the relevance of our values for the heart, the

percent of relaxation of the heart after one second, or the duration of an average heartbeat, was determined.

2.4 Histological analysis

After mechanical testing, tissue samples were immediately embedded in optimal cutting temperature (OCT) compound, frozen on dry ice and sliced on a cryostat into 5–10 μm thick sections. For immunohistochemistry (IHC), sections were fixed in 4% paraformaldehyde (PFA) for 30 min. Samples were then permeabilized for 1 h in 0.1% Triton X-100 in phosphate-buffered saline (PBS). The samples were blocked for 3–4 h in a solution of 0.3% Tween20 and 2% bovine serum albumin (BSA) in PBS. Primary antibodies were diluted in blocking solution and incubated for 1 h at room temperature, or overnight at 4 °C. Slides were washed several times with 0.1% Tween20 and 1% BSA in PBS, before incubation with the secondary antibodies diluted in blocking buffer for 1 h at room temperature. Slides were imaged using a Leica SP8 laser scanning confocal microscope with a 10 × dry, 25 × water-immersion objective and 63 × oil-immersion objective for α-smooth muscle actin (α-SMA) fiber analysis.

For Picrosirius red (PSR) staining, samples were fixed in 4% PFA for 30 min and stained in 0.1% PSR solution for 1 h at room temperature. Slides were then placed in a 0.01 N HCl solution for 2 min to wash away residual PSR. Slides were dehydrated in washes of increasing ethanol percentage and mounted with Permount mounting medium.

Oil Red O samples were fixed in 10% formalin for 30 min. The slides were then washed twice in running tap water, and dehydrated in 60% isopropanol for 2 min. They were then incubated with a 0.3% solution of Oil Red O for 2 min. Samples were then rinsed again with 60% isopropanol for 2 min, counterstained with hematoxylin and mounted with a glycerin solution.

2.5 Quantification of histology

Large scan images were quantified for area of α-SMA and α-actinin. A threshold was applied to all channels, and particle analysis was performed using ImageJ. The area of all particles found on a large scan image was summed to acquire total area for a given channel. The area of α-SMA and α-actinin was normalized to DAPI area as a proxy for expression per cell. For α-SMA stress fiber analysis, four representative 63 × images were analyzed per slide via CT-FIRE (Liu et al. 2017) with the threshold set to 1250. CT-FIRE gave us measurements for fiber width, length and straightness.

Polarized light Picrosirius red images were analyzed via CT-FIRE as well to characterize collagen fiber number, size and alignment. Brightness was adjusted in ImageJ on some images to enhance the number of fibers visible for quantification. Oil Red O images were quantified using a custom Python script (Supplemental File 1). The code used a saturation-based threshold to separate the sample from the background. The area occupied by the Oil Red O stain was then identified by pixels that fall under the HSV (hue, saturation, value) values for the colors red and pink. The rest of the sample (stained with hematoxylin) was identified by pixels with HSV corresponding to blues and purples. Using this script, the fat was quantified as the percentage of Oil Red O stained area over the total hematoxylin tissue area.

2.6 Collagen quantification

Collagen content was determined using a hydroxyproline assay. Briefly, tissue samples were frozen, lyophilized, weighed and then crushed using a pestle. The tissue was washed in PBS for 30 min, centrifuged, then dissolved in a 0.5 M acetic acid and 1 mg/mL pepsin solution and stirred overnight at 4 °C. Resultant tissue was centrifuged at 21,000 g for 30 min, and separated into pellet and supernatant. The supernatant was eluted to a new tube and placed on a hot plate at 105 °C until only solid remained. Both tubes were mixed with 6 M HCl and heated to 105 °C overnight. Sample solution was isolated, mixed with isopropanol and incubated in 1:4 chloramine T and acetate citrate buffer for 10 min. Samples were then mixed with Ehrlich's reagent and isopropanol (3:13) and incubated at 58 °C for 30 min. The reaction was halted with ice, and absorbance was read at 558 nm on Synergy H1 multi-mode microplate reader.

2.7 Statistical analysis

Normality of distribution was determined visually through Q–Q plots and histograms of the dataset. Human cardiac tissue $\tau_{1/2}$ data were non-normally distributed, as opposed to the porcine tissue which appeared normally distributed. Statistical analysis of human tissue was conducted via Kruskal–Wallis test for analysis between three or more groups, or Mann–Whitney test between two groups. All other data were statistically analyzed using one-way ANOVA or Student's *t*-test. All data are represented as mean ± standard deviation.

3 Results

3.1 Porcine tissue was fast relaxing throughout all myocardial layers

To test our hypothesis that cardiac tissue is fast relaxing, the porcine LV was isolated and characterized histologically and mechanically (Fig. 1). We found aligned α-actinin

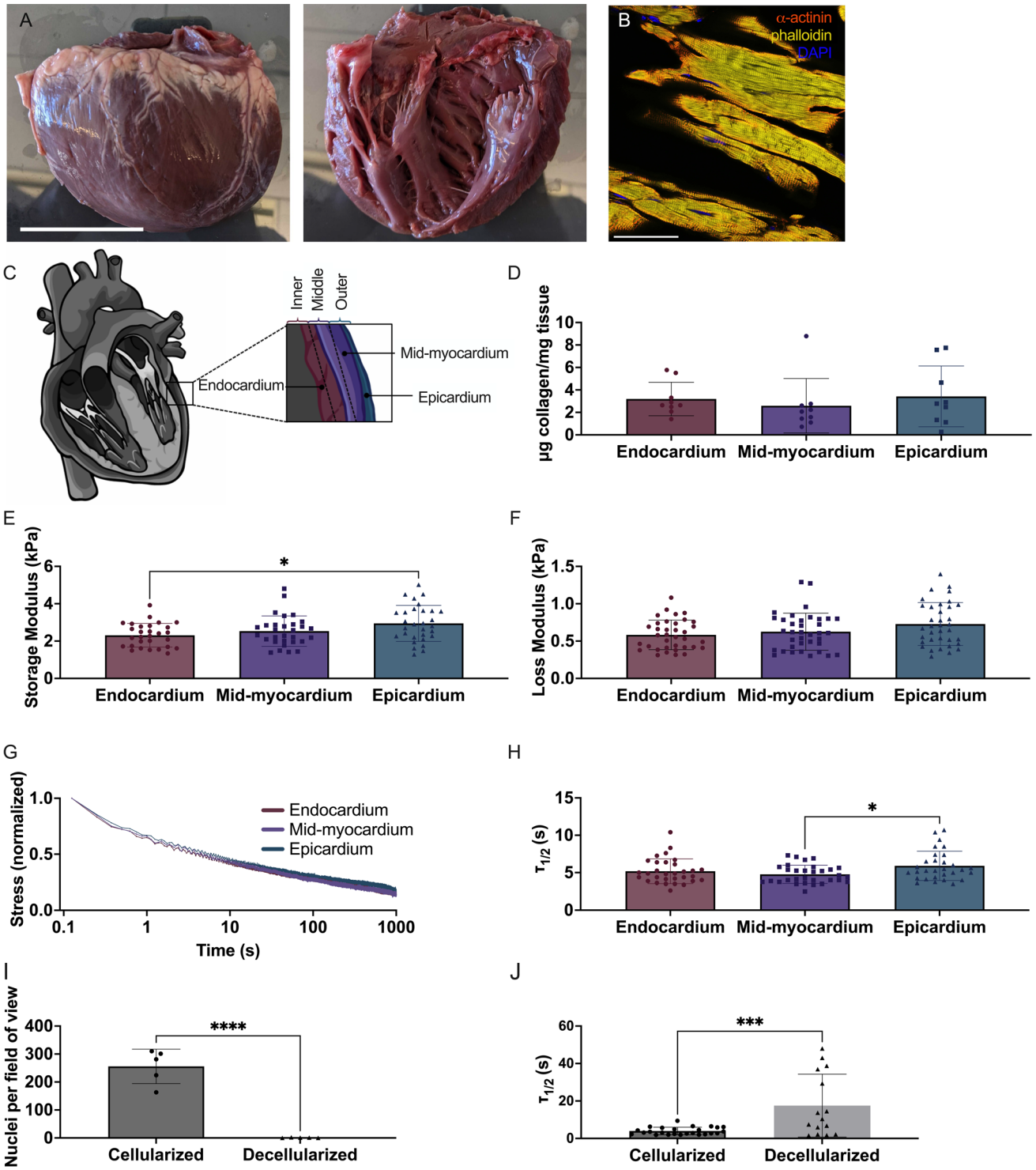

Fig. 1 Porcine LV exhibits fast stress relaxation throughout all heart layers. **A** Gross image of excised porcine LV. **B** Immunohistochemistry image of porcine tissue stained for α-actinin (red). **C** Schematic of different layers of the heart. **D** Collagen content for each layer of the porcine LV was quantified via hydroxyproline assay. **E** Storage Moduli, **F** Loss Moduli, **G** Stress relaxation curves and **H** and $\tau_{1/2}$ were measured on the rheometer. **I** Porcine tissue was decellularized, verified by a depletion of DAPI. **J** Viscoelasticity of cellularized and decellularized tissue was measured on the microindenter. Data are represented as mean ± standard deviation. Only statistics with p value less than or equal to 0.05 are shown. *$p \leq 0.05$, ***$p \leq 0.001$, ****$p \leq 0.0001$

positive CMs (Fig. 1B), as well as a consistent concentration of approximately 3 µg collagen/mg tissue within each cardiac layer (Fig. 1C, D). The storage modulus for all tissue layers was also very similar, around 2.5 kPa, with a slight increase in the average storage modulus for the epicardium at 2.9 kPa (Fig. 1E). There was no significant difference in the loss modulus between layers, which were all around 0.6 kPa. Taken together, our measurements of the storage and loss moduli indicate limited differences in viscoelasticity between tissue layers, with only a slight difference between the endocardium and epicardium (Fig. 1E, F). During stress relaxation tests, all layers of the tissue relaxed very rapidly, reaching $\tau_{1/2}$ in less than 6 s; corresponding well with our original hypothesis that cardiac tissue is fast relaxing. To determine the speed of relaxation, we quantified the $\tau_{1/2}$, or the time it takes for the stress to reach half of its maximum value. Interestingly, epicardium tissue relaxed roughly a full second slower than the other layers, at 5.9 s (Fig. 1G, H).

3.2 Decellularized porcine myocardium relaxed slower than cellularized porcine myocardium

We successfully decellularized the tissue, finding a significant depletion of nuclei in the decellularized tissue (Supplemental Fig. 1A, B, 1I). We measured the $\tau_{1/2}$ values for the cellularized tissue and decellularized tissue on the microindenter. We found that cellularized tissue relaxed significantly faster than decellularized, at an average $\tau_{1/2}$ of 3.9 s, while decellularized tissue had an average $\tau_{1/2}$ of 17.5 s (Fig. 1J).

3.3 Stress relaxation tests performed via rheometry or microindentation yield similar trends in $\tau_{1/2}$ values

We compared $\tau_{1/2}$ values obtained from stress relaxation tests performed in compression mode on both the microindenter and rheometer. LV tissue from the same pigs was used for both. However, since these tests are destructive to the tissue, the same tissue samples were not used for both measurements. There was a significant difference in the values, with the microindenter recording significantly faster $\tau_{1/2}$ values at 2.7 s compared to the rheometer at 5.5 s (Supplemental Fig. 2). Although this was a significant discrepancy, the difference between the average of the two measurements was less than 3 s. Previous studies have shown that $\tau_{1/2}$ values of tissue can have differences as large as 100–1000 s depending on tissue type (Chaudhuri et al. 2016) and pathology (Fan et al. 2024; Rubiano et al. 2018).

3.3.1 Ischemic heart failure tissue exhibited slower stress relaxation in the endocardium and faster stress relaxation in the epicardium

Information on patients within each group is summarized in Table 1. For each patient, both the endocardium and epicardium of the LV were tested. The average stress relaxation curves for the endocardium indicated that non-failing tissues relaxed faster than non-ischemic and ischemic HF (Fig. 2A). We used this data to quantify the time at which the stress reached half its maximum values, or $\tau_{1/2,}$ and found that non-failing was significantly faster than ischemic HF (Fig. 2C). However, epicardium showed the opposite trend, with the ischemic HF group exhibiting the fastest stress relaxation (Fig. 2B), and the $\tau_{1/2}$ data were in agreement, indicating ischemic HF was significantly faster than non-ischemic HF and non-failing (Fig. 2D). We also compared the $\tau_{1/2}$ values of endocardium and epicardium between each group and found a significant difference in the endocardium and epicardium in the ischemic groups (Supplemental Fig. 3). To justify why stress relaxation is important to consider for cardiac function, we analyzed the amount of relaxation that occurred within one second, the approximate time frame it takes to complete one human cardiac cycle. We found substantial stress relaxation occurred in just one second, with 35–40% of the initial stress relaxing on average in all groups, and significant decreases in percent of stress relaxation between non-failing and non-ischemic HF in the endocardium (Supplemental Fig. 4).

3.3.2 Endocardial and epicardial tissues were categorized based on relaxation time into either slow, fast or extremely fast categories

We plotted the $\tau_{1/2}$ values as a density plot to visualize the spread of the data and categorized the samples based on their viscoelasticity into either fast or slow relaxing tissues (Fig. 2E). Moving forward, this separation of data based on stress relaxation allowed us to determine which biological differences were correlated to changes in stress relaxation.

Table 1 Patient demographics of indented cardiac tissue

Group	Age (years)	Sex (M/F)	Body mass index	Endo average $\tau_{1/2}$ (s)	Epi average $\tau_{1/2}$ (s)
Non-failing ($n=5$)	50.1 ± 9.7	3/2	30.9 ± 6.4	12.1 ± 19.9	14.6 ± 23.0
Non-ischemic HF($n=5$)	48.3 ± 9.6	3/2	29.5 ± 7.5	15.6 ± 27.1	11.3 ± 16.3
Ischemic HF($n=5$)	50.3 ± 8.1	3/2	26.2 ± 2.7	15.8 ± 21.1	4.3 ± 3.8

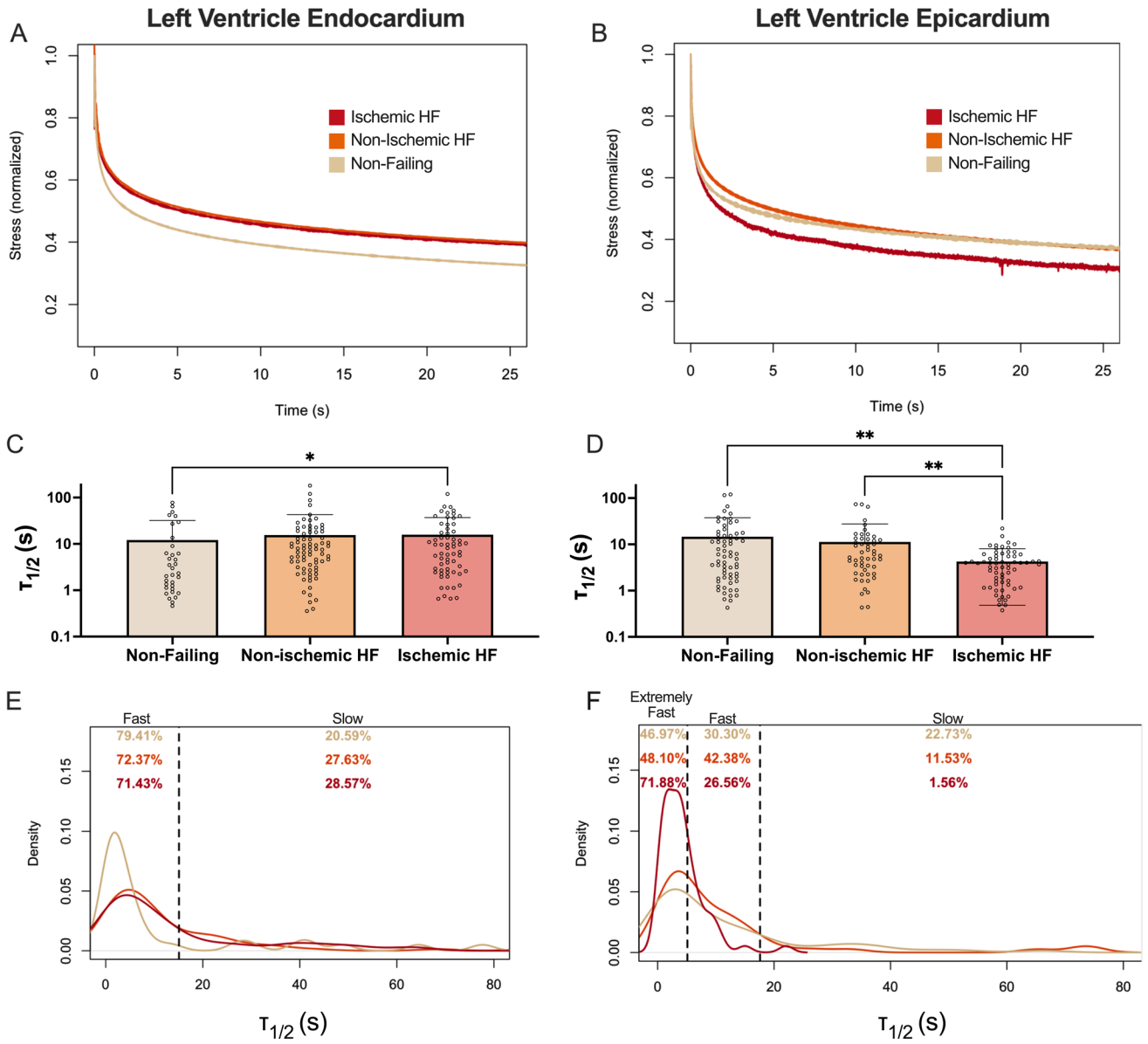

Fig. 2 Analysis of stress relaxation times reveals differences in HF in the endocardium and epicardium. Average stress relaxation graphs for non-failing, ischemic and non-ischemic human tissue for **A** LV endocardium and **B** LV epicardium ($n=5$ patients per group). Time at which stress reaches half the maximum value, or $\tau_{1/2}$, for **C** LV endocardium and **D** LV epicardium. Each data point corresponds to one indentation measurement. Density graphs of $\tau_{1/2}$ values for **E** LV endocardium, **F** LV epicardium. Dotted lines represent from left to right: reported $\tau_{1/2}$ values for fat (only in epicardium graph) and the average plus six standard deviations from the porcine tissue in Fig. 1. Percentages indicate percent of data located between dotted lines. Data are represented as mean ± standard deviation. Only statistics with p value less than or equal to 0.05 are shown. $^{*}p \leq 0.05$, $^{**}p \leq 0.01$

We derived cutoff points using the average $\tau_{1/2}$ of the porcine data plus 6 standard deviations to capture the heterogeneity in the human data. The cutoff values for fast relaxing tissue were 15.14 s for the endocardium and 17.65 s for the epicardium; samples with $\tau_{1/2}$ values greater than those cutoffs were considered slow relaxing. In the endocardium data, we found that there was a distinct peak in fast $\tau_{1/2}$ values for the non-failing data that fell within the fast relaxing regime, encompassing 79.41% of the data, while the ischemic and non-ischemic data had broader peaks with lower percentages within the fast relaxing range (72.37 and 71.43%, respectively) (Fig. 2E). We hypothesized that fat was responsible for the fast stress relaxation of the epicardium. In order to explore this further, we introduced another cutoff point based on the $\tau_{1/2}$ of adipose tissue reported in the literature at 5.12 s (Gefen and Haberman 2007). This separation allowed us to determine if fat deposition correlated with fast stress relaxation. We termed the values

faster than 5.12 s extremely fast. The density plot of the epicardium showed that 71.88% of values for the ischemic HF group fall in the extremely fast category, compared with only 48.1% of non-ischemic HF and 46.97% of non-failing tissue samples. Additionally, the ischemic HF group had almost no samples (1.56%) within the slow relaxing regime, while non-failing tissue had the highest amount of slow stress relaxation values at 22.73%, followed by non-ischemic with 11.53% (Fig. 2F). While the tissue samples were classified by patient status, there will be heterogeneity within the tissue samples from each patient. Samples from failing hearts will not be consistently pathological, and there could be regions of fibrosis in samples from non-failing hearts. To account for this heterogeneity and focus on our analysis on the tissue viscoelasticity, throughout the rest of the paper we will refer to the samples using the following categories for endocardium: fast ($\tau_{1/2} < 15.14$ s), and slow relaxing ($\tau_{1/2} > 15.14$ s); and for epicardium: extremely fast ($\tau_{1/2} < 5.12$ s), fast ($5.12\text{ s} < \tau_{1/2} < 17.65$ s) and slow relaxing ($\tau_{1/2} > 17.65$ s).

3.4 α-actinin and α-SMA are increased in fast relaxing tissues

To correlate stress relaxation rates with tissue disease state, we stained indented tissue samples for α-actinin, a cytoskeletal actin-binding protein that is present in CMs, and α-SMA, a protein present in activated myofibroblasts. When analyzing the data based on the clinical categories, we saw no significant differences in α-actinin or α-SMA area (Supplemental Fig. 5). Therefore, we separated the data based on their stress relaxation times established in Fig. 2E, F.

Qualitatively, we saw stark differences in *α*-actinin area between fast and slow relaxing groups in both endocardium and epicardium. In the endocardium, the fast relaxing tissue had the most *α*-actinin, indicating the highest presence of CMs, while the slow relaxing tissue had far less *α*-actinin staining, and the *α*-actinin positive CMs present appeared smaller in length and diameter. However, there did not seem to be perceptible differences in *α-SMA* staining. (Fig. 3A). The epicardium showed similar staining of *α*-actinin and *α-SMA* between tissues that were fast and slow relaxing. In the extremely fast relaxing group, we found a lack of staining for both *α-SMA* and *α*-actinin, indicating a lack of musculature (Fig. 3B).

Upon quantifying the images, we found that α-actinin area was significantly greater in fast relaxing versus slow relaxing endocardium tissue (Fig. 3C). The epicardium showed a significant increase in *α*-actinin stained area in fast relaxing tissue compared to extremely fast, and comparable amounts in slow relaxing (Fig. 3D). We found significantly increased *α-SMA* staining in fast relaxing endocardial tissue compared to slow relaxing tissue (Fig. 3E). In the epicardium, there was a trend of increasing α-SMA staining in fast relaxing tissue compared to slow, but it was non-significant (Fig. 3F).

3.5 Slow relaxing endocardium contained larger α-SMA fibers

We were able to visualize α-SMA fibers in all stress relaxation groups in both the epicardium and endocardium (Fig. 4A, B). α-SMA fibers are considered a more accurate representation of activated cardiac fibroblasts compared to α-SMA presence alone (Bretherton et al. 2020). Therefore, we quantified α-SMA fiber formation to determine if there was any difference in cardiac fibroblast activation between groups. Within the endocardium, *α-SMA* stress fibers were significantly thicker in slow relaxing tissue ($0.24\ \mu m \pm 0.0064\ \mu m$) compared to fast ($0.23\ \mu m \pm 0.0052\ \mu m$) (Fig. 4D) and more aligned (0.91 ± 0.004 versus 0.90 ± 0.005) (Fig. 4G). However, there was no significant difference in fiber length (Fig. 4C), or number (Fig. 4H) in slow relaxing tissues compared to fast relaxing tissue. In the epicardium, we found no significant differences between the quantified α-SMA stress fibers with relationship to stress relaxation of the tissue (Fig. 4E, F, I, J). However, we saw a trend of increased fiber number in the fast relaxing group, indicating more activated fibroblasts compared to slow and extremely fast groups.

3.6 Slow relaxing endocardium exhibited increased collagen staining and collagen fiber size

We stained the samples with Picrosirius red and imaged them under polarized light to visualize the collagen fibers (Rittié 2017). Within the endocardium, we observed trends of increasing collagen amount in slower relaxing tissues. Qualitatively, the images in Fig. 5A display more and brighter polarized collagen fibers in the slow relaxing group. In the epicardium, polarized light Picrosirius red images revealed greater collagen abundance in the fast relaxing group compared to extremely fast and slow relaxing tissues (Fig. 5B). We found a significant increase in red pixels in these polarized images in slow relaxing endocardium tissue, denoting increased collagen amount, while in the epicardium the fast relaxing tissues exhibited higher number of red pixels (Fig. 5C, E). These results were in agreement with the hydroxyproline assay, which showed increasing collagen in slower relaxing endocardium and fast relaxing epicardium (Fig. 5D, F).

Through CT-FIRE analysis, we found that in the endocardium, collagen fibers were significantly longer and thicker in slower relaxing tissue than the faster relaxing tissues (Fig. 5G, H). However, we found no significant differences in fiber straightness or fiber number between groups, although there was a distinct trend for increased fiber number in slow relaxing tissues (Fig. 5K, L). In the epicardium,

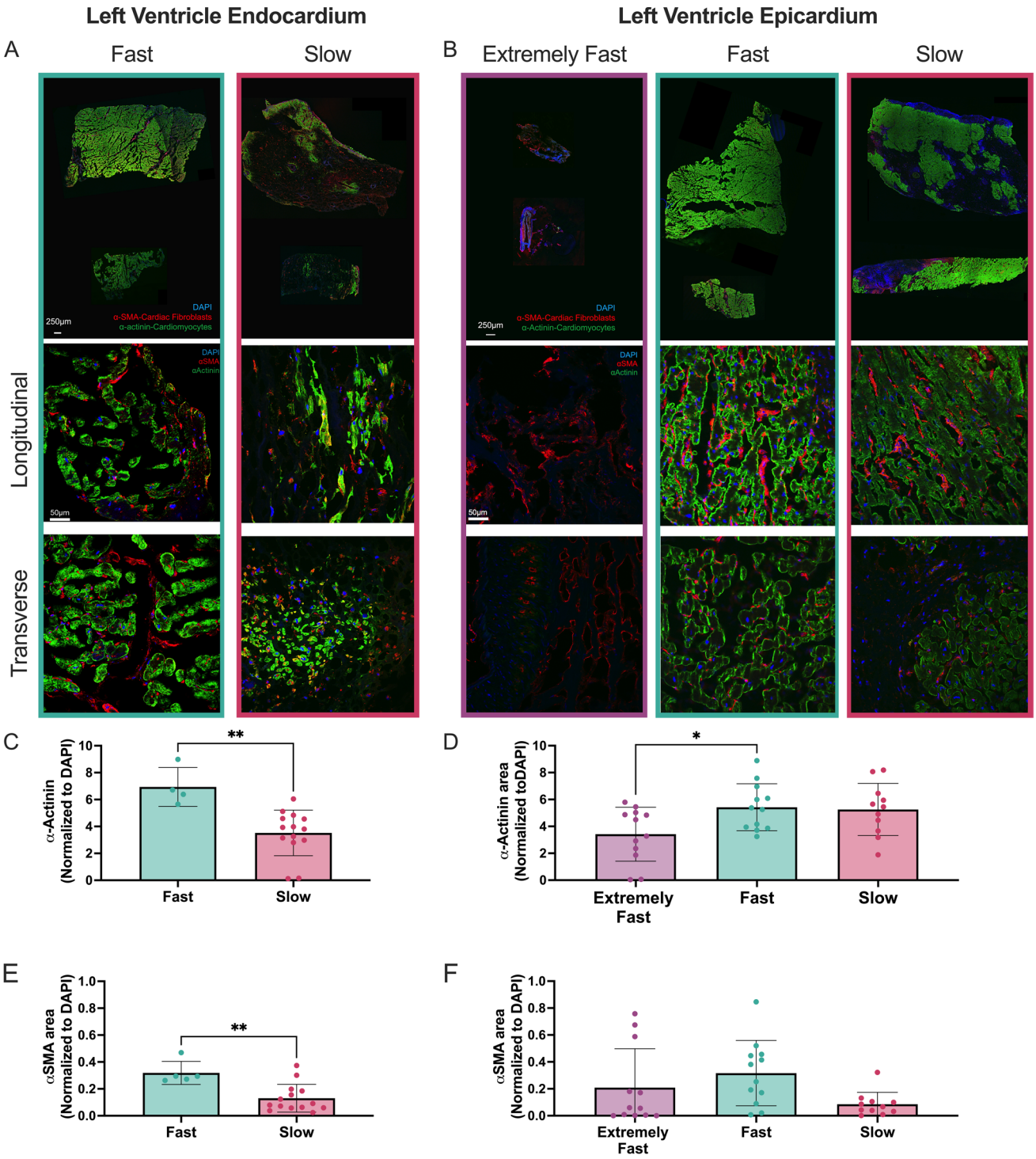

Fig. 3 Fast relaxing tissue shows increased α-actinin and α-smooth muscle actin (α-SMA) in the endocardium and epicardium. **A**, **B** Representative large scans, and 25× images of longitudinal and transverse sections of endocardial and epicardial tissues within the extremely fast, fast and slow relaxing categories. Images were stained with DAPI in blue, *α*-actinin in green and *α-SMA* in red. Brightness and contrast on extremely fast epicardium large scan were increased more than others for better visualization. **C**, **D** Quantification of the area of *α*-actinin normalized to DAPI. **E**, **F** Quantification of the area of *α-SMA* normalized to DAPI. Each data point corresponds to one tissue sample. Data are represented as mean ± standard deviation. Only statistics with p value less than or equal to 0.05 are shown. *$p \leq 0.05$, **$p \leq 0.01$

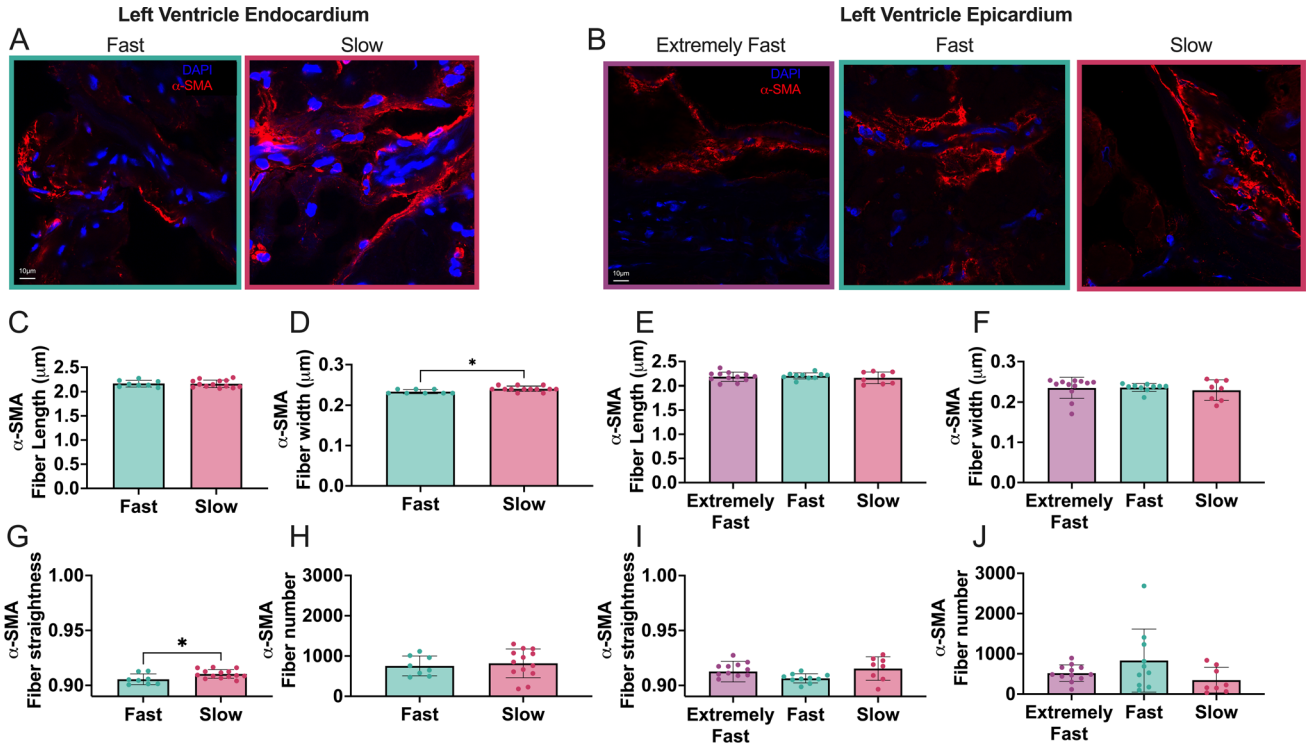

Fig. 4 *α-SMA* stress fibers are thicker and straighter in slow relaxing endocardium tissue but show no significant trends in the epicardium. **A**, **B** 63×magnification images of *α-SMA* in extremely fast, fast and slow relaxing tissue of the endocardium and epicardium. Images were analyzed for α-SMA stress fiber **C**, **E** length, **D**, **F** width and **G**, **H** straightness. Graphs on the left represent endocardium, graphs on the right are epicardium. Each data point corresponds to one tissue sample. Data are represented as mean ± standard deviation. Only statistics with p value less than or equal to 0.05 are shown. $^*p \leq 0.05$

there was no significance in collagen fiber length, width, straightness or number (Fig. 5I, J, M, N).

3.7 Epicardial tissue exhibited increased Oil Red O staining compared to the endocardium

We found that all epicardium tissues relaxed significantly faster than the endocardium, with epicardial tissue exhibiting an average $\tau_{1/2}$ of 10.1 s compared to an average $\tau_{1/2}$ of 15.0 s for endocardium (Supplemental Fig. 6). We hypothesized that fat, which is known to be fast relaxing, was contributing to this difference. Although patient data were anonymized and deidentifiable, we knew which patients were diabetic and therefore likely had more epicardial fat (Li et al. 2019). We analyzed our $\tau_{1/2}$ values based on patients with or without diabetes (Supplemental Fig. 7A). Interestingly, in the endocardium we observed that patients with diabetes had significantly faster $\tau_{1/2}$, with a mean of 9.1 s, compared to those without diabetes, which exhibited a mean $\tau_{1/2}$ of 18.7 s. In the epicardium, we observed similar trends, although they were not significant (Supplemental Fig. 7B).

We then stained for lipids using Oil Red O to identify fat deposits in the tissue. Both fast and slow relaxing endocardium had limited Oil Red O staining (Fig. 6A). However, the epicardium had substantially more in all groups, especially the extremely fast and fast relaxing tissues (Fig. 6B). By quantifying the Oil Red O stain, we found that the aggregation of all epicardium groups had significantly higher amounts of fat than the aggregation of all epicardium groups (Fig. 6C). When separating by stress relaxation times, we found the extremely fast, fast and slow epicardium had significantly higher Oil red O staining than the slow relaxing endocardium. There was also a trend of faster relaxing epicardium exhibiting higher average Oil Red O staining than slower relaxing epicardium, although this was not statistically significant (Fig. 6D).

4 Discussion

We have shown, through mechanical tests, that viscoelasticity changes with respect to disease state within the heart. We then used histological and biochemical analysis of collagen and fat to correlate local tissue composition and structure with stress relaxation. Although there have been notable viscoelastic measurements of cardiac tissue previously, both directly (Hassan et al. 2012; Pinto and Fung 1973; Chaturvedi et al. 2010; Islam et al. 2020; Liu et al.

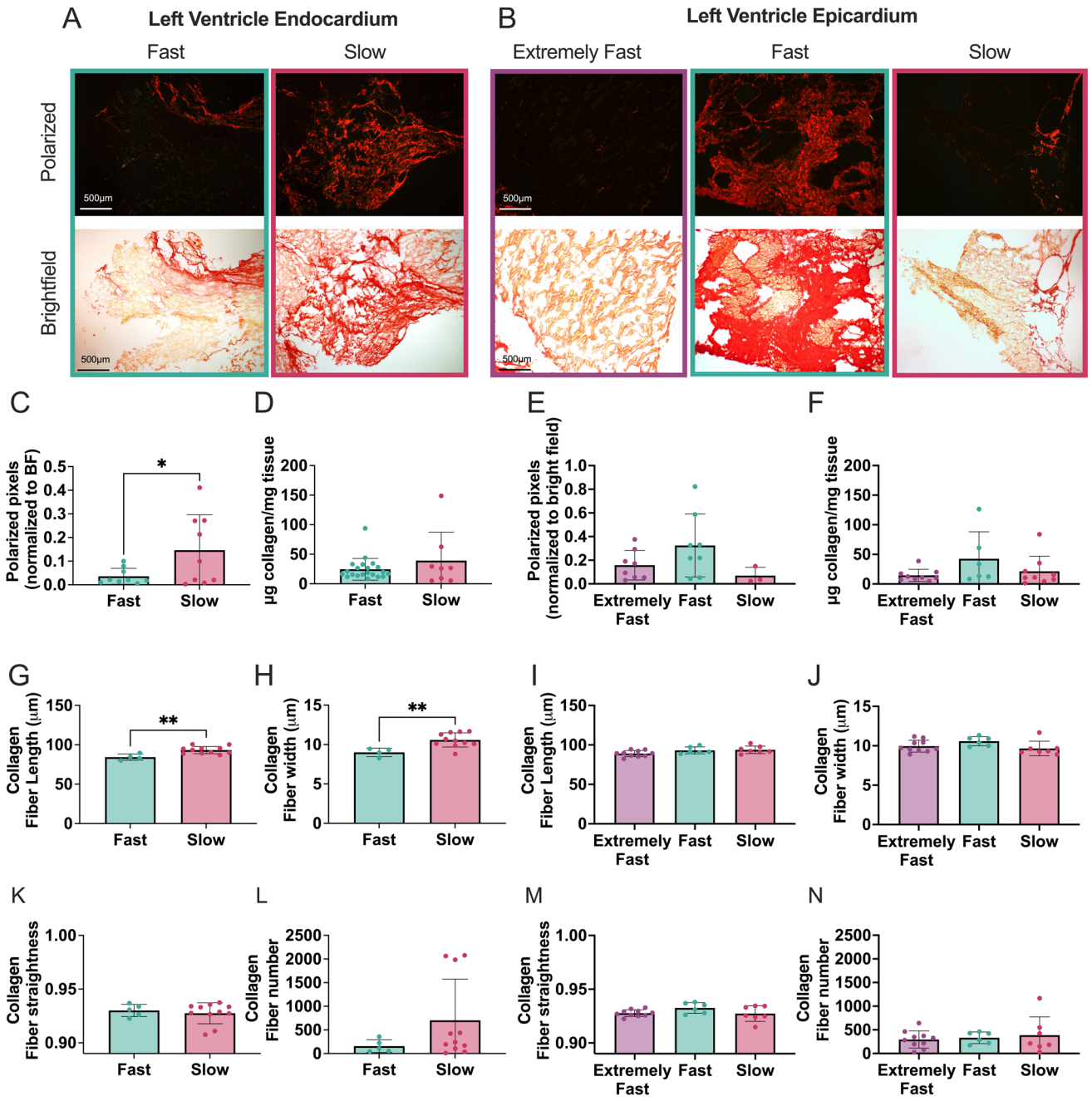

Fig. 5 Collagen analysis shows increased fibrosis in slow relaxing endocardium but no significance in the epicardium. **A, B** Representative Picrosirius red polarized and bright field images from endocardium and epicardium categorized as either extremely fast, fast or slow relaxing. Analysis of polarized pixels normalized to bright field area in (**C**) endocardium and **E** epicardium. **D**, **F** Hydroxyproline assay quantification of collagen concentration in tissue samples. Quantification of collagen fibers in Picrosirius polarized light images, including **G**, **I** fiber length, **H**, **J** fiber width, **K**, **M** fiber straightness and (LN) fiber number. Each data point corresponds to one tissue sample. Data are represented as mean ± standard deviation. Only statistics with p value less than or equal to 0.05 are shown. *$p \leq 0.05$, **$p \leq 0.01$

2021; Kakaletsis et al. 2021) and indirectly through imaging modalities (Kanai 2005; Villalba-Orero et al. 2021), these measurements are difficult to translate to in vitro and in silico models. Several cardiac tissue measurements are conducted on custom-built instruments, making it difficult to reproduce viscoelastic measurements on other instruments. These tests also vary in the type of test performed, including stress relaxation, creep or oscillating stress, and if the force is applied in compression, tension or shear. This concern is best demonstrated by a prior study comparing different mechanical measurement methods for the same cell source, resulting in material parameter estimations that

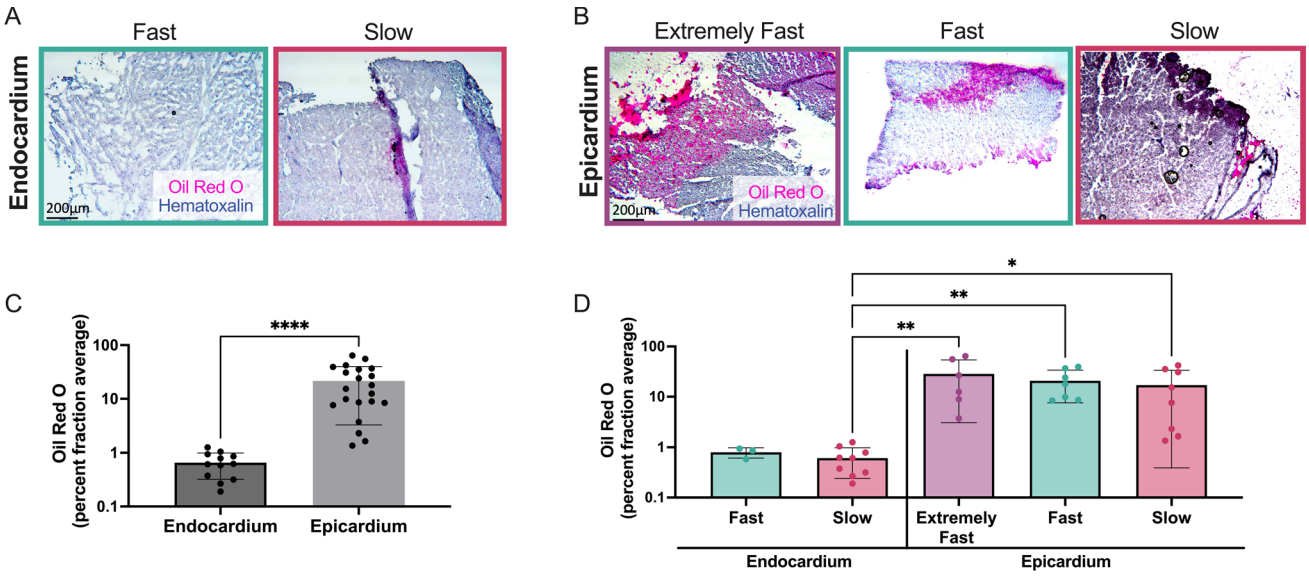

Fig. 6 Oil Red O staining is upregulated in extremely fast relaxing epicardium. **A**, **B** Representative Oil red O stain from endocardium (left) and epicardium (right). **C** Quantification of Oil Red O stain for endocardium and epicardium. **D** Quantification of Oil red O separated based on stress relaxation speed for both endocardium and epicardium. Each data point corresponds to one tissue sample. Data are represented as mean ± standard deviation. Only statistics with p value less than or equal to 0.05 are shown. *$p \leq 0.05$, **$p \leq 0.01$, ****$p \leq 0.0001$

were orders of magnitude apart across methods (Wu et al. 2018). Although we found it necessary to use a specialized instrument for our studies, due to small specimen size, we validated our measurements on a commercially available rheometer. We further conducted a simple compression stress relaxation test at 10% strain that can be replicated by several commercially available instruments including a rheometer, Instron or dynamic mechanical analyzer. Sample species, myopathy, storage and preparation can also lead to variation in reported results. Our HF and non-failing cardiac samples were acquired from a reputable human biobank, increasing the likelihood that our samples would produce relevant results (Blair et al. 2016).

Porcine hearts were highly viscoelastic (~5 s), relaxing much faster than other soft tissues (~100 s–1000 s) (Chaudhuri et al. 2016; Remache et al. 2018; Pioletti and Rakotomanana 2000). When decellularized, the tissue became slower relaxing (17.5 s), suggesting that both cells and ECM contribute to the viscoelastic response. Our data are in agreement with previous studies that have shown that microtubules and sarcomeres within CMs (Land et al. 2017; LeBar et al. 2024; Tombe and Keurs 1992; Stuyvers et al. 1997) as well as cardiac ECM (Stroud et al. 2002) are viscoelastic. These data counter studies that determined the characteristic relaxation time of the heart to be 600 s, based on a fit to a Maxwell element model, which is far too long to be relevant at a heartbeat scale (Hassan et al. 2012). Contrary to their findings, we found that even within 1 s, the tissue relaxes around 40%, which likely influences cardiac function (Supplemental Fig. 4).

We found faster relaxing tissue had more *α-SMA*, which was in agreement with in vitro studies showing fast relaxing hydrogels induce increased *α-SMA* expression in myofibroblasts (Ma et al. 2020). However, activated cardiac fibroblasts are known to not only express *α-SMA*, but form *α-SMA* stress fibers when fully differentiated (Bretherton et al. 2020). We found a trend of increasing *α-SMA* stress fiber number in slower relaxing tissue, indicating more activated fibroblasts. We also found significant increases in fiber width and alignment in slow relaxing tissues. Our reported differences in the stress fibers are a unique finding, since there is little quantitative data within the literature on stress fiber size and alignment in cardiac tissue. Previous in vitro studies have only qualitatively noted that fibroblasts stress fiber thickness changes due to substrate properties, with fibroblasts on silicone exhibiting thinner fibers than those on plastic (Hinz et al. 2001).

In the epicardium, fat serves a number of vital functions. However, excessive accumulation of epicardial fat can contribute to HF (Wu et al. 2017; Li et al 2019). We found that increases in fat and decreases in CMs led to faster tissue stress relaxation, likely contributing to further dysregulation of heart function. It is known that different cell types can exhibit distinct mechanical properties; therefore, it is likely that this change in cell populations, regardless of matrix remodeling, has a direct impact on the stress relaxation rate (Darling et al. 2008).

A limitation of this work is that we could only mechanically characterize the heart tissue in the passive state, since

our tests were performed ex vivo, and thus, our measurements are most relevant to diastole. During contraction, the activation of cross bridges within the CMs changes the tissues stiffness, and likely changes tissue viscoelasticity (Campbell et al. 2003). Additionally, the heterogeneous nature of cardiac tissue was an expected challenge within this study. For example, scarring associated with HF is not usually present throughout all of the heart (Bourantas et al. 2011). To address tissue heterogeneity, we compared the biochemical and histological data from each tissue sample based on its $\tau_{1/2}$ value. This analysis yielded significant differences between fast and slow relaxing tissues, compared to classifying the data based on the clinical categorization which showed no significance (Supplemental Fig. 5). Patient-to-patient variability was another challenge, as we only had access to 5 patients in each group. Even with our limited sample size, we showed that comorbidities can influence cardiac viscoelasticity. Our data indicated that diabetic patients, across HF and non-HF groups, had faster relaxing epicardium (Supplemental Fig. 7). Investigation into what other patient characteristics effect viscoelasticity could lead to interesting insights into cardiac disease.

5 Conclusion

We have shown that both human and porcine hearts are fast relaxing through direct stress relaxation tests on ex vivo tissue. Our studies further conclude that, across all groups, the endocardium becomes slower relaxing during HF due to fibrosis. The epicardium, however, shows a reverse trend, becoming faster relaxing during HF due to increased fat deposition. These results have important implications for computational and biomaterial cardiac disease modeling.

Supplementary Information The online version contains supplementary material available at https://doi.org/10.1007/s10237-024-01909-4.

Acknowledgements Special thanks to Ahmed Al Kindi for assisting in microindentation studies.

Author contributions Marissa Gionet-Gonzales was involved in conceptualization, methodology, software, validation, formal analysis, investigation, writing—original draft, visualization and project administration. Gianna Gathman contributed to software, validation, formal analysis, investigation, writing—review and editing and visualization. Jonah Rosas took part in methodology, validation and investigation. Kyle Y. Kunisaki was responsible for methodology, investigation and writing—review and editing. Dominique Gabriele P. Inocencio and Niki Hakami were involved in methodology and investigation. Gregory N. Milburn took part in methodology and supervision. Angela A. Pitenis and Kenneth S. Campbell took part in resources, supervision and writing—review and editing. Beth L. Pruitt and Ryan S. Stowers formal analysis were involved in conceptualization, resources, supervision, writing—review and editing and funding acquisition.

Funding MGG acknowledges funding from American Heart Association (DOI https://doi.org/10.58275/AHA.24POST1195931.pc.gr.190777), National Science Foundation (NSF) (ID 769-2075), and the Presidents Postdoctoral Fellowship Program. G.G. acknowledges support from the National Institutes of Health (NIH 1T32GM141846). This work was additionally supported by NIH grant RM131981, as well as funding from the NSF (CMM1 1662431). Rheological data was acquired through the MRL Shared Experimental Facilities, which are supported by the MRSEC Program of the NSF under Award No. DMR 2308708; a member of the NSF-funded Materials Research Facilities Network (www.mrfn.org). Microindenter supplies and consumables used in this work were partially supported by the NSF Materials Research Science and Engineering Center (MRSEC) at UC Santa Barbara through DMR-2308708 (IRG-2). J.M.R. acknowledges academic year support from the Gates Millennium Scholarship through the Bill and Melinda Gates Foundation and Hispanic Scholarship Fund and summer support from the NSF CAREER Award (CMMI-CAREER-2048043). A.A.P. acknowledges summer support from the NSF CAREER Award (CMMI-CAREER-2048043) and from the Army's Institute for Collaborative Biotechnologies UARC Contract W911NF-19-2-0026). K.S.C. and G.N.M. acknowledge support from NIH R01HL148785. B.L.P. acknowledges funding from NSF CMMI BRITE 2227509.

Data availability The data generated during the current study are available from the corresponding author upon request.

Declarations

Conflict of interest The authors declare no competing interests.

Open Access This article is licensed under a Creative Commons Attribution 4.0 International License, which permits use, sharing, adaptation, distribution and reproduction in any medium or format, as long as you give appropriate credit to the original author(s) and the source, provide a link to the Creative Commons licence, and indicate if changes were made. The images or other third party material in this article are included in the article's Creative Commons licence, unless indicated otherwise in a credit line to the material. If material is not included in the article's Creative Commons licence and your intended use is not permitted by statutory regulation or exceeds the permitted use, you will need to obtain permission directly from the copyright holder. To view a copy of this licence, visit http://creativecommons.org/licenses/by/4.0/.

References

Atkins DJ, Rosas JM, Månsson LK, Shahverdi N, Dey SS, Pitenis AA (2024) Survival-associated cellular response maintained in pancreatic ductal adenocarcinoma (PDAC) switched between soft and stiff 3D microgel culture. ACS Biomater Sci Eng 10(4):2177–2187. https://doi.org/10.1021/acsbiomaterials.3c01079

Bakunts K, Gillum N, Karabekian Z, Sarvazyan N (2008) Formation of cardiac fibers in Matrigel matrix. Biotechniques 44(3):341–348. https://doi.org/10.2144/000112682

Bauer A, Gu L, Kwee B, Li WA, Dellacherie M, Celiz AD, Mooney DJ (2017) Hydrogel substrate stress-relaxation regulates the spreading and proliferation of mouse myoblasts. Acta Biomater 62:82–90. https://doi.org/10.1016/j.actbio.2017.08.041

Blair CA, Haynes P, Campbell SG, Chung C, Mitov MI, Dennis D, Bonnell MR, Hoopes CW, Guglin M, Campbell KS (2016) A protocol for collecting human cardiac tissue for research. VAD J. https://doi.org/10.13023/VAD.2016.12

Boothe SD, Myers JD, Pok S, Sun J, Xi Y, Nieto RM, Cheng J, Jacot JG (2016) The effect of substrate stiffness on cardiomyocyte action potentials. Cell Biochem Biophys 74(4):527–535. https://doi.org/10.1007/s12013-016-0758-1

Bourantas CV, Nikitin NP, Loh HP, Lukaschuk EI, Sherwi N, de Silva R, Tweddel AC, Alamgir MF, Wong K, Gupta S et al (2011) Prevalence of scarred and dysfunctional myocardium in patients with heart failure of ischaemic origin: a cardiovascular magnetic resonance study. J Cardiovasc Magn Reson 13(1):53. https://doi.org/10.1186/1532-429X-13-53

Bretherton R, Bugg D, Olszewski E, Davis J (2020) Regulators of cardiac fibroblast cell state. Matrix Biol 91–92:117–135. https://doi.org/10.1016/j.matbio.2020.04.002

Cameron AR, Frith JE, Cooper-White JJ (2011) The influence of substrate creep on mesenchymal stem cell behaviour and phenotype. Biomaterials 32(26):5979–5993. https://doi.org/10.1016/j.biomaterials.2011.04.003

Campbell KS, Patel JR, Moss RL (2003) Cycling cross-bridges increase myocardial stiffness at submaximal levels of Ca2+ activation. Biophys J 84(6):3807–3815. https://doi.org/10.1016/S0006-3495(03)75108-X

Caporizzo MA, Prosser BL (2021) Need for speed: the importance of physiological strain rates in determining myocardial stiffness. Front Physiol 12:696694. https://doi.org/10.3389/fphys.2021.696694

Chang ACY, Pardon G, Chang ACH, Wu H, Ong S-G, Eguchi A, Ancel S, Holbrook C, Ramunas J, Ribeiro AJS et al (2021) Increased tissue stiffness triggers contractile dysfunction and telomere shortening in dystrophic cardiomyocytes. JSCR 16(9):2169–2181. https://doi.org/10.1016/j.stemcr.2021.04.018

Charrier EE, Pogoda K, Wells RG, Janmey PA (2018) Control of cell morphology and differentiation by substrates with independently tunable elasticity and viscous dissipation. Nat Commun 9(1):449. https://doi.org/10.1038/s41467-018-02906-9

Chaturvedi RR, Herron T, Simmons R, Shore D, Kumar P, Sethia B, Chua F, Vassiliadis E, Kentish JC (2010) Passive stiffness of myocardium from congenital heart disease and implications for diastole. Circulation 121(8):979–988. https://doi.org/10.1161/CIRCULATIONAHA.109.850677

Chau AL, Getty PT, Rhode AR, Bates CM, Hawker CJ, Pitenis AA (2022) Superlubricity of pH-responsive hydrogels in extreme environments. Frontiers Chem. https://doi.org/10.3389/fchem.2022.891519

Chau AL, Edwards CER, Helgeson ME, Pitenis AA (2023) Designing superlubricious hydrogels from spontaneous peroxidation gradients. ACS Biomater Sci Eng 15(36):43075–43086. https://doi.org/10.1021/acsami.3c04636

Chaudhuri O, Gu L, Darnell M, Klumpers D, Bencherif SA, Weaver JC, Huebsch N, Mooney DJ (2015) Substrate stress relaxation regulates cell spreading. Nat Commun 6(1):6365. https://doi.org/10.1038/ncomms7365

Chaudhuri O, Gu L, Klumpers D, Darnell M, Bencherif SA, Weaver JC, Huebsch N, Lee HP, Lippens E, Duda GN et al (2016) Hydrogels with tunable stress relaxation regulate stem cell fate and activity. Nat Mater 15(3):326–334. https://doi.org/10.1038/nmat4489

Corbin EA, Vite A, Peyster EG, Bhoopalam M, Brandimarto J, Wang X, Bennett AI, Clark AT, Cheng X, Turner KT et al (2019) Tunable and reversible substrate stiffness reveals a dynamic mechanosensitivity of cardiomyocytes. ACS Appl Mater Interfaces 11(23):20603–20614. https://doi.org/10.1021/acsami.9b02446

Darling EM, Topel M, Zauscher S, Vail TP, Guilak F (2008) Viscoelastic properties of human mesenchymally-derived stem cells and primary osteoblasts, chondrocytes, and adipocytes. J Biomech 41(2):454–464. https://doi.org/10.1016/j.jbiomech.2007.06.019

de Tombe PP, ter Keurs HE (1992) An internal viscous element limits unloaded velocity of sarcomere shortening in rat myocardium. J Physiol 454:619–642. https://doi.org/10.1113/jphysiol.1992.sp019283

Fan W, Adebowale K, Váncza L, Li Y, Rabbi MF, Kunimoto K, Chen D, Mozes G, Chiu DK, Tao J et al (2024) Matrix viscoelasticity promotes liver cancer progression in the pre-cirrhotic liver. Nature 626(7999):635–642. https://doi.org/10.1038/s41586-023-06991-9

Gandhi SK, Powers JC, Nomeir AM, Fowle K, Kitzman DW, Rankin KM, Little WC (2001) The pathogenesis of acute pulmonary edema associated with hypertension. New England J Med 344(1):17–22. https://doi.org/10.1056/NEJM200101043440103

Gefen A, Haberman E (2007) Viscoelastic properties of ovine adipose tissue covering the gluteus muscles. J Biomech Eng 129(6):924–930. https://doi.org/10.1115/1.2800830

Gong Z, Szczesny SE, Caliari SR, Charrier EE, Chaudhuri O, Cao X, Lin Y, Mauck RL, Janmey PA, Burdick JA et al (2018) Matching material and cellular timescales maximizes cell spreading on viscoelastic substrates. Proc Natl Acad Sci U S A 115(12):E2686–E2695. https://doi.org/10.1073/pnas.1716620115

Hassan MA, Hamdi M, Noma A (2012) The nonlinear elastic and viscoelastic passive properties of left ventricular papillary muscle of a guinea pig heart. J Mech Behav Biomed Mater 5(1):99–109. https://doi.org/10.1016/j.jmbbm.2011.08.011

Haynes P, Nava KE, Lawson BA, Chung CS, Mitov MI, Campbell SG, Stromberg AJ, Sadayappan S, Bonnell MR, Hoopes CW et al (2014) Transmural heterogeneity of cellular level power output is reduced in human heart failure. J Mol Cell Cardiol 72:1–8. https://doi.org/10.1016/j.yjmcc.2014.02.008

Hegyi B, Shimkunas R, Jian Z, Izu LT, Bers DM, Chen-Izu Y (2021) Mechanoelectric coupling and arrhythmogenesis in cardiomyocytes contracting under mechanical afterload in a 3D viscoelastic hydrogel. Proc Nat Acad Sci. https://doi.org/10.1073/pnas.2108484118

Hess OM, Grimm J, Krayenbuehl HP (1979) Diastolic simple elastic and viscoelastic properties of the left ventricle in man. Circ 59(6):1178–1187. https://doi.org/10.1161/01.cir.59.6.1178

Hinz B, Celetta G, Tomasek JJ, Gabbiani G, Chaponnier C (2001) Alpha-smooth muscle actin expression upregulates fibroblast contractile activity. Mol Biol Cell 12(9):2730–2741. https://doi.org/10.1091/mbc.12.9.2730

Hunter JD, Hancko A, Shakya P, Hill R, Saviola AJ, Hansen KC, Davis ME, Christman KL (2022) Characterization of decellularized left and right ventricular myocardial matrix hydrogels and their effects on cardiac progenitor cells. J Mol Cell Cardiol 171:45–55. https://doi.org/10.1016/j.yjmcc.2022.06.007

Islam MR, Virag J, Oyen ML (2020) Micromechanical poroelastic and viscoelastic properties of ex-vivo soft tissues. J Biomech 113:110090. https://doi.org/10.1016/j.jbiomech.2020.110090

Kaiser NJ, Kant RJ, Minor AJ, Coulombe KLK (2019) Optimizing blended collagen-fibrin hydrogels for cardiac tissue engineering with human iPSC-derived cardiomyocytes. ACS Biomater Sci Eng 5(2):887–899. https://doi.org/10.1021/acsbiomaterials.8b01112

Kakaletsis S, Meador WD, Mathur M, Sugerman GP, Jazwiec T, Malinowski M, Lejeune E, Timek TA, Rausch MK (2021) Right ventricular myocardial mechanics: multi-modal deformation, microstructure, modeling, and comparison to the left ventricle. Acta Biomater 123:154–166. https://doi.org/10.1016/j.actbio.2020.12.006

Kanai H (2005) Propagation of spontaneously actuated pulsive vibration in human heart wall and in vivo viscoelasticity estimation. IEEE Trans Ultrason, Ferroelectr Freq Control 52(11):1931–1942. https://doi.org/10.1109/TUFFC.2005.1561662

Körner A, Mosqueira M, Hecker M, Ullrich ND (2021) Substrate stiffness influences structural and functional remodeling in induced pluripotent stem cell-derived cardiomyocytes. Front Physiol 12:710619. https://doi.org/10.3389/fphys.2021.710619

Krick BA, Vail JR, Persson BNJ, Sawyer WG (2012) Optical in situ micro tribometer for analysis of real contact area for contact mechanics, adhesion, and sliding experiments. Tribol Lett 45(1):185–194. https://doi.org/10.1007/s11249-011-9870-y

Land S, Park-Holohan SJ, Smith NP, Dos Remedios CG, Kentish JC, Niederer SA (2017) A model of cardiac contraction based on novel measurements of tension development in human cardiomyocytes. J Mol Cell Cardiol 106:68–83. https://doi.org/10.1016/j.yjmcc.2017.03.008

LeBar K, Liu W, Chicco AJ, Wang Z (2024) Role of microtubule network in the passive anisotropic viscoelasticity of healthy right ventricle. J Biomech Eng. https://doi.org/10.1115/1.4064685

Li Y, Liu B, Jing X, Deng S, Yan Y, She Q (2019) Epicardial fat tissue in patients with diabetes mellitus: a systematic review and meta-analysis. Cardiovasc Diabetol 18(1):3. https://doi.org/10.1186/s12933-019-0807-3

Liu Y, Keikhosravi A, Mehta GS, Drifka CR, Eliceiri KW (2017) Methods for quantifying fibrillar collagen alignment. Methods Mol Biol 1627:429–451. https://doi.org/10.1007/978-1-4939-7113-8_28

Liu W, Nguyen-Truong M, Ahern M, Labus KM, Puttlitz CM, Wang Z (2021) Different passive viscoelastic properties between the left and right ventricles in healthy adult ovine. J Biomech Eng. https://doi.org/10.1115/1.4052004

Ma H, Macdougall LJ, Gonzalez Rodriguez A, Schroeder ME, Batan D, Weiss RM, Anseth KS (2020) Calcium signaling regulates valvular interstitial cell alignment and myofibroblast activation in fast-relaxing boronate hydrogels. Macromol Biosci 20(12):e2000268. https://doi.org/10.1002/mabi.202000268

Magder S (2016) Volume and its relationship to cardiac output and venous return. Crit Care 20(1):271. https://doi.org/10.1186/s13054-016-1438-7

Mendiola EA, Neelakantan S, Xiang Q, Merchant S, Li K, Hsu EW, Dixon RAF, Vanderslice P, Avazmohammadi R (2023) Contractile adaptation of the left ventricle post-myocardial infarction: predictions by rodent-specific computational modeling. Ann Biomed Eng 51(4):846–863. https://doi.org/10.1007/s10439-022-03102-z

Ott HC, Matthiesen TS, Goh SK, Black LD, Kren SM, Netoff TI, Taylor DA (2008) Perfusion-decellularized matrix: using nature's platform to engineer a bioartificial heart. Nat Med 14(2):213–221. https://doi.org/10.1038/nm1684

Pinto JG, Fung YC (1973) Mechanical properties of the heart muscle in the passive state. J Biomech 6(6):597–616. https://doi.org/10.1016/0021-9290(73)90017-1

Pioletti DP, Rakotomanana LR (2000) On the independence of time and strain effects in the stress relaxation of ligaments and tendons. J Biomech 33(12):1729–1732. https://doi.org/10.1016/s0021-9290(00)00128-7

Pislaru C, Urban MW, Pislaru SV, Kinnick RR, Greenleaf JF (2014) Viscoelastic properties of normal and infarcted myocardium measured by a multifrequency shear wave method: comparison with pressure-segment length method. Ultrasound Med Biol 40(8):1785–1795. https://doi.org/10.1016/j.ultrasmedbio.2014.03.004FromScienceDirect

Rawat H, Kornherr J, Zawada D, Bakhshiyeva S, Kupatt C, Laugwitz KL, Bähr A, Dorn T, Moretti A, Nowak-Imialek M (2023) Recapitulating porcine cardiac development. Front Cell Dev Biol 11:1111684. https://doi.org/10.3389/fcell.2023.1111684

Remache D, Caliez M, Gratton M, Dos Santos S (2018) The effects of cyclic tensile and stress-relaxation tests on porcine skin. J Mech Behav Biomed Mater 77:242–249. https://doi.org/10.1016/j.jmbbm.2017.09.009

Rittié L (2017) Method for picrosirius red-polarization detection of collagen fibers in tissue sections. Methods Mol Biol 1627:395–407. https://doi.org/10.1007/978-1-4939-7113-8_26

Roman B, Kumar SA, Allen SC, Delgado M, Moncayo S, Reyes AM, Suggs LJ, Chintalapalle R, Li C, Joddar B (2021) A model for studying the biomechanical effects of varying ratios of collagen types I and III on cardiomyocytes. Cardiovasc Eng Technol 12(3):311–324. https://doi.org/10.1007/s13239-020-00514-7

Roshanbinfar K, Schiffer M, Carls E, Angeloni M et al (2024) Electrically conductive collagen-PEDOT:PSS hydrogel prevents post-infarct cardiac arrhythmia and supports hiPSC-cardiomyocyte function. Adv Mater. https://doi.org/10.1002/adma.202403642

Rubiano A, Delitto D, Han S, Gerber M, Galitz C, Trevino J, Thomas RM, Hughes SJ, Simmons CS (2018) Viscoelastic properties of human pancreatic tumors and in vitro constructs to mimic mechanical properties. Acta Biomater 67:331–340. https://doi.org/10.1016/j.actbio.2017.11.037

Rysä J, Tokola H, Ruskoaho H (2018) Mechanical stretch induced transcriptomic profiles in cardiac myocytes. Sci Rep 8(1):4733. https://doi.org/10.1038/s41598-018-23042-w

Sacco JL, Vaneman ZT, Gomez EW (2024) Extracellular matrix viscoelasticity regulates TGFβ1-induced epithelial-mesenchymal transition and apoptosis via integrin linked kinase. J Cell Physiol 239(2):e31165. https://doi.org/10.1002/jcp.31165

Schmitt PR, Dwyer KD, Minor AJ, Coulombe KLK (2022) Wet-spun polycaprolactone scaffolds provide customizable anisotropic viscoelastic mechanics for engineered cardiac tissues. Polymers 14(21):4571. https://doi.org/10.3390/polym14214571

Stroud JD, Baicu CF, Barnes MA, Spinale FG, Zile MR (2002) Viscoelastic properties of pressure overload hypertrophied myocardium: effect of serine protease treatment. Am J Physiol Heart Circ Physiol 282(6):H2324-2335. https://doi.org/10.1152/ajpheart.00711.2001

Stuyvers BDMY, Miura M, ter Keurs HEDJ (1997) Dynamics of viscoelastic properties of rat cardiac sarcomeres during the diastolic interval: involvement of Ca2+. J Physiol 502(3):661–677. https://doi.org/10.1111/j.1469-7793.1997.661bj.x

Tikenoğulları OZ, Costabal FS, Yao J, Marsden A, Kuhl E (2022) How viscous is the beating heart? Insights from a computational study. Comput Mech 70(3):565–579. https://doi.org/10.1007/s00466-022-02180-z

Urueña JM, Hart SM, Hood DL, McGhee EO, Niemi SR, Schulze KD, Levings PP, Sawyer WG, Pitenis AA (2018) Considerations for biotribometers: cells, gels, and tissues. Tribol Lett 66(4):141. https://doi.org/10.1007/s11249-018-1094-y

Vetter FJ, McCulloch AD (1998) Three-dimensional analysis of regional cardiac function: a model of rabbit ventricular anatomy. Prog Biophys Mol Biol 69(2–3):157–183. https://doi.org/10.1016/s0079-6107(98)00006-6

Villalba-Orero M, Jiménez-Riobóo RJ, Gontán N, Sanderson D, López-Olañeta M, García-Pavía P, Desco M, Lara-Pezzi E, Gómez-Gaviro MV (2021) Assessment of myocardial viscoelasticity with Brillouin spectroscopy in myocardial infarction and aortic stenosis models. Sci Rep 11(1):21369. https://doi.org/10.1038/s41598-021-00661-4

Willems R, Janssens KLPM, Bovendeerd PHM, Verhoosel CV, van der Sluis O (2024) An isogeometric analysis framework for ventricular cardiac mechanics. Comput Mech 73(3):465–506. https://doi.org/10.1007/s00466-023-02376-x

Wong TY, Juang WC, Tsai CT, Tseng CJ, Lee WH, Chang SN, Cheng PW (2018) Mechanical stretching simulates cardiac physiology and pathology through mechanosensor piezo1. J Clin Med 7(11):410. https://doi.org/10.3390/jcm7110410

Wu Y, Zhang A, Hamilton DJ, Deng T (2017) Epicardial fat in the maintenance of cardiovascular health. Methodist Debakey Cardiovasc J 13(1):20–24. https://doi.org/10.14797/mdcj-13-1-20

Wu PH, Aroush DR, Asnacios A, Chen WC, Dokukin ME, Doss BL, Durand-Smet P, Ekpenyong A, Guck J, Guz NV et al (2018) A comparison of methods to assess cell mechanical properties. Nat Methods 15(7):491–498. https://doi.org/10.1038/s41592-018-0015-1

Zhang W, Jilberto J, Sommer G, Sacks MS, Holzapfel GA, Nordsletten DA (2023) Simulating hyperelasticity and fractional

viscoelasticity in the human heart. Comput Methods Appl Mech and Eng 411:116048. https://doi.org/10.1016/j.cma.2023.116048
Zile MR, Brutsaert DL (2002) New concepts in diastolic dysfunction and diastolic heart failure: part I: diagnosis, prognosis, and measurements of diastolic function. Circ 105(11):1387–1393. https://doi.org/10.1161/hc1102.105289

Publisher's Note Springer Nature remains neutral with regard to jurisdictional claims in published maps and institutional affiliations.